Polymer Chemistry

ROYAL SOCIETY OF CHEMISTRY

PAPER

View Article Online
View Journal | View Issue



Cite this: *Polym. Chem.*, 2025, **16**, 2757

# Programming cascade mesophase transitions of enzyme-responsive formulations *via* molecular engineering of dendritic amphiphiles†

Krishna Vippala,[a,b,c] Nicole Edelstein-Pardo,[a,b,d] Shahar Tevet,[a,b,f] Parul Rathee,[a,b,d] Gil Koren,[b,d,e] Roy Beck[b,d,e] and Roey J. Amir[*a,b,d,f]

The ability to program cascades of enzymatically induced transitions of polymeric assemblies across various mesophases holds promise for developing new dynamic materials with complex response mechanisms, mimicking the intricate behavior of proteins and other biological systems. In this study, we demonstrate the feasibility of controlling the rates of such sequential transitions by molecular engineering of the polymeric building blocks. To this end, we utilized a hydrogel forming PEG-based tri-block amphiphile (TBA) and micelles forming di-block amphiphiles (DBAs), composed of dendrons with enzymatically cleavable ester end-groups as their hydrophobic blocks, to create co-assembled nano-micellar formulations. We investigated their multi-step mesophase transitions, first from micelles into macroscopic hydrogels and subsequently into water-soluble polymers, in the presence of the activating enzyme porcine liver esterase (PLE). To demonstrate the ability to control the time frame of the micelle-to-hydrogel mesophase transition, we designed and synthesized three DBAs with varying dendritic architectures and degrees of hydrophobicity. These DBAs are composed of hydrophobic dendrons with two, three, and four lipophilic end-groups, designated as DBA-C6×2, DBA-C6×3, and DBA-C6×4, respectively. Our results indicated that the co-assembled micelles containing the least hydrophobic DBA-C6×2 rapidly transformed into a hydrogel within less than two hours upon exposure to PLE. In contrast, the micellar formulation with the most hydrophobic DBA-C6×4 took over two days to transition into the hydrogel mesophase. These findings underscore the potential of using molecular engineering to tailor the behavior of programable polymeric assemblies.

Received 2nd December 2024,
Accepted 13th May 2025

DOI: 10.1039/d4py01378f

rsc.li/polymers



## Introduction

The remarkable ability of various assembled nano-, micro-, and macro-structures in nature to respond and adapt to environmental cues has remained a steadfast source of inspiration for scientific innovation. One realm in which this inspiration has yielded transformative outcomes is the development of stimuli-responsive polymeric amphiphiles and their self-assemblies, a burgeoning field with extensive applications.[1–8] Within this domain, variations in pH, high concentrations of molecular species (*e.g.* reactive oxygen species, glutathione, *etc.*), and enzymes, have served as potent triggers for the activation of responsive materials.[9–12] Among the various types of responsive systems, enzyme-responsive ones can potentially endow researchers with a profound level of control, enabling precise modulation of structural alterations within polymeric assemblies to facilitate a wide spectrum of functions, including drug delivery and depot formation.[12–16]

At the heart of the design of enzyme-responsive polymers and assemblies lies the art of programming materials to react selectively to the specific enzymes. This feat is accomplished through the strategic integration of enzyme-responsive components into the polymeric amphiphiles that compose the responsive systems.[17–20] However, unlike biological systems, most reported synthetic enzyme-responsive systems are capable of transitioning only between two states, and only limited examples of systems that can transition between more than two states have been reported. These multi-states systems

[a]*Department of Organic Chemistry, School of Chemistry, Faculty of Exact Sciences, Tel-Aviv University, Tel-Aviv 6997801, Israel. E-mail: amirroey@tauex.tau.ac.il*
[b]*Tel-Aviv University Center for Nanoscience and Nanotechnology, Tel-Aviv University, Tel-Aviv, 6997801, Israel*
[c]*Analytical Technologies Unit R&D, Teva Pharmaceutical Industries, Kfar Saba 4410202, Israel*
[d]*The Center for Physics and Chemistry of Living Systems, Tel-Aviv University, Tel-Aviv 6997801, Israel*
[e]*School of Physics and Astronomy, Faculty of Exact Sciences, Tel-Aviv University, Tel-Aviv 6997801, Israel*
[f]*The ADAMA Center for Novel Delivery Systems in Crop Protection, Tel-Aviv University, Tel-Aviv, 6997801, Israel*
† Electronic supplementary information (ESI) available. See DOI: https://doi.org/10.1039/d4py01378f

are based on the incorporation of several enzyme-responsive components into the polymeric backbone of the amphiphiles.[21,22] Recently, we demonstrated a different strategy to program enzyme-responsive micellar formulation to undergo sequential multi-mesophase transitions in response to enzymatic activation.[23,24] Our strategy was based on co-assembling hydrogel forming tri-block amphiphile (TBA) and stabilizing di-block amphiphile (DBA), both featuring identical esterase-responsive or amide-responsive groups in their hydrophobic dendron, into nano-sized micelles. While the DBA accounts for the stabilization of a micellar state for the mixed formulation, its selective enzymatic degradation in the presence of the activating enzyme, due to its faster unimer-micelle exchange rate, results in the transformation of the TBA into hydrogel mesophase. In the second stage, the TBA based hydrogel is slowly degraded by the same activating enzyme into water-soluble polymers.

The transition from micelles to hydrogel mesophase is governed by the hydrolysis rate of the stabilizing DBA. It's noteworthy that enzymes can cleave the end-groups in the DBA dendrons only when the amphiphiles are in their unimer-form rather than as micelles.[25] Thus, adjusting the hydrophilic-lipophilic ratio of the DBA by modifying the hydrophobicity of the dendron should lead to a change in the DBA hydrolysis rate, as it influences the equilibrium between the unimer and micelles. The hydrophobicity of the dendron can be changed by either extending the aliphatic chain length,[26] or by changing the number of arms in the dendron.[27] In this work, we synthesized three distinct DBA variants with different dendritic architectures by altering the number of enzymatically cleavable dendritic end-groups, and evaluated the impact of this engineered change in hydrophobicity on the rates of enzymatically induced DBA-hydrolysis and hydrogel formation.

These mixed micellar formulations may be beneficial for potential biomedical applications due to the ability to transition between the three mesophases—micelles, hydrogel, and soluble hydrophilic polymers. For instance, while the micellar phase can be easily administered due to its low viscosity and the nano-size dimensions of micelles,[28–30] the *in situ* formation of a slowly degrading hydrogel phase can be explored for its potential to serve as a degradable drug depot for sustained release.[31–39] Hence, studying the underlying mechanisms that influence the kinetics of this cascade of multi-mesophase transitions—from nano-sized micelles to macroscopic gels and eventually into soluble polymers—could not only enhance our understanding of how nature adapts to external stimuli but also potentially aid in designing more advanced drug delivery systems.

## Results and discussion

### Design and synthesis of DBA and TBA

The design of DBAs was based on $PEG_{5kDa}$-dendron hybrids, which due to their high modularity and structural precision, can be tuned to achieve the desired number of dendritic end-groups by simply altering the central branching unit (Scheme 1). The synthesis for all three DBAs initiated with conjugating an amine functionalized $mPEG_{5kDa}$-$NH_2$, synthesized following previously reported procedures,[27] with dendritic branching units of different multiplicities. For the DBA with two-arm dendron, 5 kDa mPEG-$NH_2$ was conjugated to 3,5-bis(allyloxy)benzoic acid,[40] serving as an $AB_2$ branching unit, using *N*,*N*′-diisopropylcarbodiimide (DIC) and OxymaPure in the presence of *N*,*N*-diisopropylethylamine (DIPEA). This reaction quantitatively yielded $mPEG_{5kDa}$-di-allyl, which was subsequently reacted by thiol–ene reaction[41] with an excess of 2-mercaptoethanol and 2,2-dimethoxy-2-phenylacetophenone (DMPA) as photo-initiator under UV irradiation at 365 nm, to obtain mPEG-diol. Finally, the obtained mPEG-diol was reacted by Steglich esterification with excess of hexanoic acid using *N*,*N*′-dicyclohexylcarbodiimide (DCC), and 4-dimethylaminopyridine (4-DMAP), to obtain the desired di-arm amphiphiles $mPEG_{5kDa}$-C6×2 (DBA-C6×2).

Similarly, the three-arm dendritic DBA was synthesized by conjugating $mPEG_{5kDa}$-$NH_2$ with 3,4,5-tris(allyloxy)benzoic acid,[27] which served as an $AB_3$ branching unit, to obtain $mPEG_{5kDa}$-tri-allyl. This compound was further reacted with an excess of 2-mercaptoethanol and DMPA under UV irradiation by thiol–ene reaction to yield mPEG-triol, followed by Steglich esterification with excess of hexanoic acid using DCC and DMPA to yield the three-arm amphiphile $mPEG_{5kDa}$-C6×3 (DBA-C6×3). For the four-arm containing DBA, $mPEG_{5kDa}$-$NH_2$ was reacted with 3,5-bis(prop-2-yn-1-yloxy) benzoic acid,[27] serving as an $AB_4$ branching unit, using DIC, OxymaPure, and DIPEA to obtain $mPEG_{5kDa}$-di-yne. Subsequently, thiol–yne reaction[42] with an excess of 2-mercaptoethanol using a catalytic amount of DMPA under UV irradiation led to the formation of mPEG-tetraol, followed by Steglich esterification with excess of hexanoic acid using DCC and DMAP to yield the desired four-arm amphiphile $mPEG_{5kDa}$-C6×4 (DBA-C6×4).

To synthesize the tri-block copolymer, commercially available 10 kDa PEG was first refluxed in toluene with potassium hydroxide, followed by addition of propargyl bromide to yield PEG-di-yne (Scheme 2). Subsequent thiol–yne reaction with an excess of cysteamine hydrochloride, utilizing a catalytic amount of DMPA under UV irradiation yielded PEG-tetra-amine. The resulting product was then reacted with 3,5-bis(allyloxy)benzoic acid, serving as an $AB_2$ branching unit, to obtain $PEG_{10kDa}$-octa-allyl, which was further reacted with an excess of 2-mercaptoethanol using DMPA under UV irradiation *via* a thiol–ene reaction to obtain $PEG_{10kDa}$-octa-ol. Finally, similar to the synthetic procedure for the DBAs, this product was coupled by Steglich esterification with excess of hexanoic acid using DCC and DMAP to obtain the desired tri-block amphiphile C6×4-$PEG_{10kDa}$-C6×4 (TBA). To verify the conversion of synthetic steps, the purity of the products, and to confirm the amphiphiles contained the desired number of end-groups, we used $^1$H NMR spectroscopy, and HPLC. Molecular weights of the amphiphiles were determined using size exclusion chromatography (SEC, Table 1). Detailed synthetic procedures and characterization data for the four amphiphiles are provided in the ESI.†

 

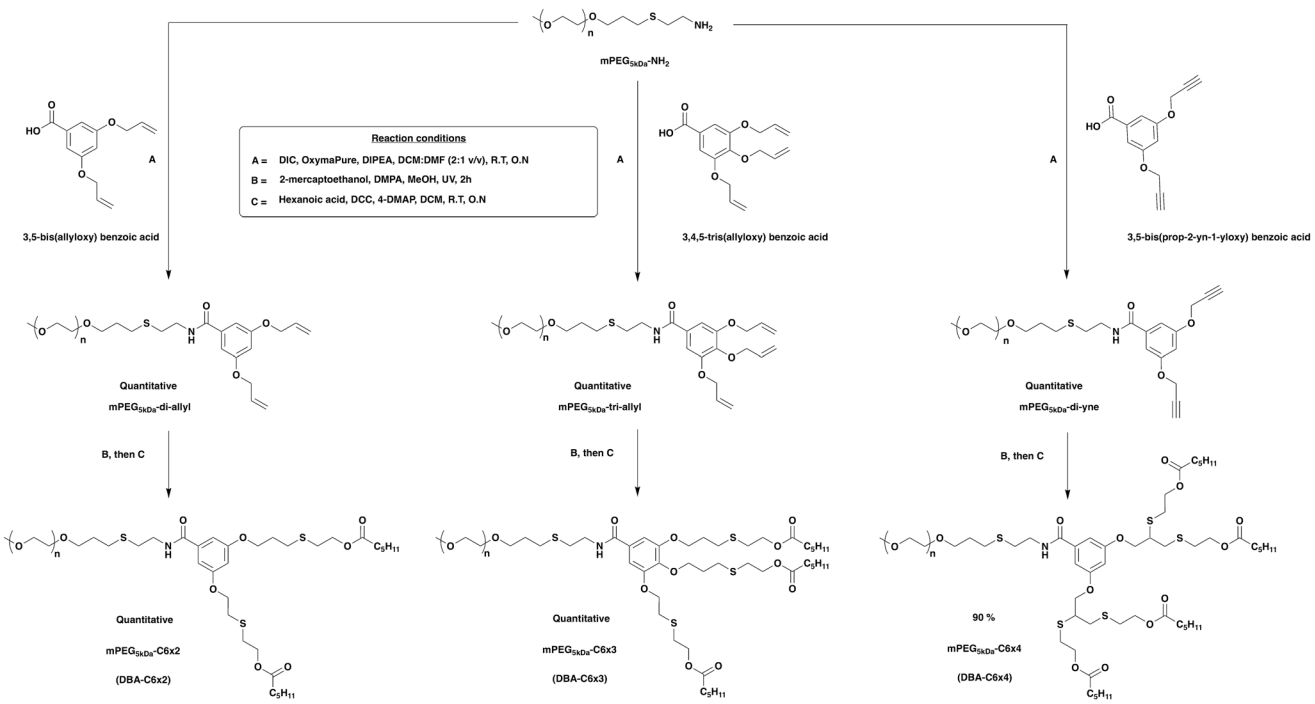


**Scheme 1** Synthetic route for DBAs with different dendritic architectures.

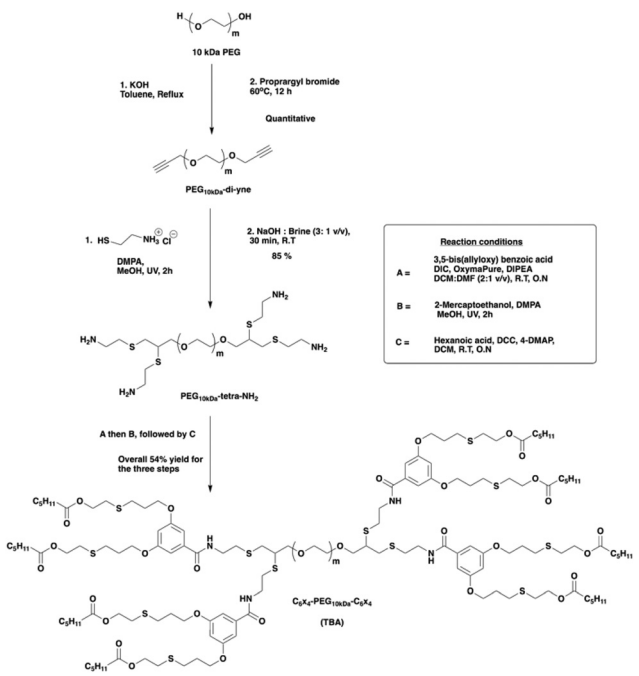


**Scheme 2** Synthetic route for making TBA.

**Table 1** Amphiphiles and their characteristics

| Amphiphile | No. of hexanoate end-groups | $M_n$[a] (Da) | $M_n$[b] (kDa) | $Đ_M$[b] |
|---|---|---|---|---|
| DBA-C6×2 | 2 | 5748 | 6.1 | 1.06 |
| DBA-C6×3 | 3 | 5980 | 6.3 | 1.05 |
| DBA-C6×4 | 4 | 6110 | 6.3 | 1.05 |
| TBA | 8 | 12 721 | 14.6 | 1.11 |

[a] $M_n$ is theoretically calculated based on assigning the molecular weights of mPEG as 5 kDa and PEG as 10 kDa. [b] $M_n$ and dispersity ($Đ_M$) were analyzed by SEC using PEG commercial standards.

### Self-assembly of DBA and TBA

After successfully synthesizing and characterizing the four amphiphiles, we initially investigated the self-assembly of the three DBAs. We first determined their critical micelle concentrations (CMC) using the Nile red method,[43] and analyzed their hydrodynamic diameters through dynamic light scattering (DLS). Notably, as can be expected, we observed that the CMC of the micelles decreased as the hydrophobicity of the underlying amphiphiles increased (Table 2). Additionally, all DBA based micelles exhibited hydrodynamic diameters of around 20 nm (DLS), and around 20–30 nm by transmission electron microscopy (TEM), which also confirmed their spheric shapes (Fig. S13†), with a slight increase in size when the hydrophobicity of the amphiphile increased (Table 2).

Next, we aimed to formulate the DBA and TBA into co-assembled micelles. Previously, we reported the feasibility of creating mixed micellar formulations at a 1 : 1 DBA to TBA weight ratio.[23,24] Henceforth, we began preparing co-assembled formulations with this ratio using our least hydrophobic DBA variant with two arms, DBA-C6×2. Briefly, DBA-C6×2 and TBA stock solutions were prepared separately by dissolving them in dichloromethane (DCM). Subsequently, the DBA-C6×2 and TBA mixtures were prepared at a 1 : 1 weight

Table 2 Formulations and their characteristics

| Formulation composition | CMC[a] (μM) | $D_H$[b] (nm) |
|---|---|---|
| DBA-C6×2 | 24 ± 2 | 18 ± 2 |
| DBA-C6×2 and TBA | 10 ± 1 | 19 ± 8 |
| DBA-C6×3 | 10 ± 1 | 19 ± 4 |
| DBA-C6×3 and TBA | 7 ± 1 | 23 ± 5 |
| DBA-C6×4 | 7 ± 1 | 21 ± 4 |
| DBA-C6×4 and TBA | 6 ± 1 | 20 ± 10 |

[a] CMC determined using the Nile red method. [b] Hydrodynamic diameter ($D_H$) of micelles measured by DLS. Micelles were made by co-assembling TBA and DBA in a 1 : 2 wt. ratio.

ratio, followed by evaporation of DCM, leaving behind a white solid thin film residue, which was then dried under reduced pressure for 12 hours. The dried thin film was hydrated with phosphate-buffered saline (PBS, pH 7.4), and the solution was vigorously vortexed and then sonicated for 15 minutes. However, at this ratio (5 mg $mL^{-1}$ of each amphiphile), we noticed some visible aggregates, indicating that DBA-C6×2 was unable to completely dissolve the TBA (Fig. S14†) at this ratio. To remedy this, we increased the concentration of DBA-C6×2 to 10 mg $mL^{-1}$, resulting in a final weight ratio of DBA-C6×2 to TBA of 2 : 1. At this ratio, we observed complete dissolution of TBA as clear solution was obtained, indicating the formation of DBA-C6×2 and TBA co-assembled micelles (Fig. 1C, $t$ = 0). We then used the same 2 : 1 ratio to prepare mixed micelle formulations with the other two DBAs, DBA-C6×3 and DBA-C6×4. To validate the formation of co-assembled micelles, we characterized their hydrodynamic radius using DLS and TEM, and determined their CMC with the Nile Red method, similar to the approach used for characterizing the self-assembly of DBAs.

For the least hydrophobic DBA-C6×2 amphiphile, the co-assembly with the TBA into mixed micelles appears to lower the CMC values compared to micelles consisting solely of DBA, indicating greater thermodynamic stability of the co-assembled ones. This effect was also observed for the DBA-C6×3 and DBA-C6×4 amphiphiles, although to a lower extent. We then characterized the formed micelles by DLS and TEM, and observed nearly similar hydrodynamic diameters for the co-assembled TBA and DBA, and the DBA micelles (Table 2, Fig. 1D and S13†).

### Formation of TBA based hydrogel

To initiate the mesophase transition, the activating enzyme porcine liver esterase (PLE, 0.5 U $mL^{-1}$), which can cleave the hydrophobic ester-containing end-groups, was added to the solution of the DBA-C6×2 and TBA co-assembled micelles, and HPLC was used to directly analyze the molecular composition of the solution at given time points. The rate of disappearance of the DBA-C6×2 and the rate of formation of hydrolyzed-DBA were calculated by measuring the area under the curve of the respective peaks in the HPLC chromatogram (Fig. 1A and B). In parallel, we used a spectrophotometer to measure the optical density of the solution at 600 nm. As the enzymatically

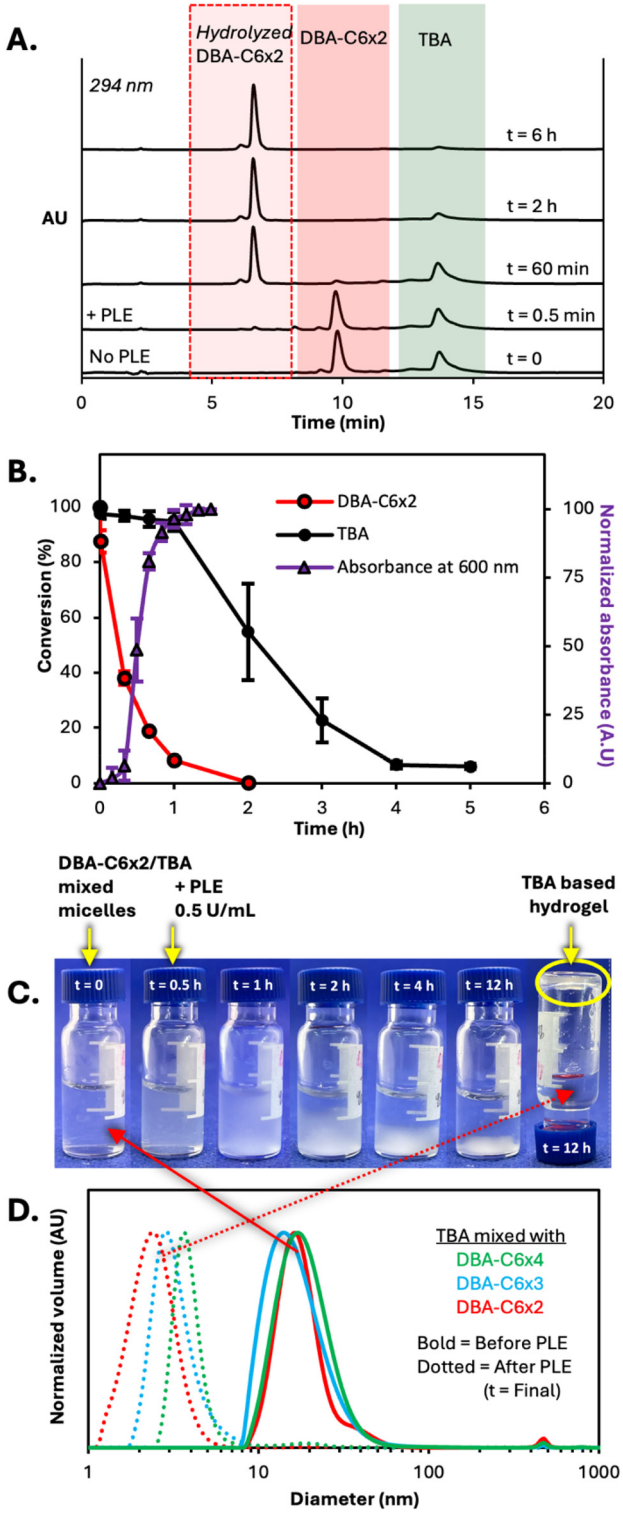


Fig. 1 (A) HPLC overlay for micelles of DBA-C6×2 (10 mg $mL^{-1}$) and TBA (5 mg $mL^{-1}$) over time in the presence of PLE (0.5 U $mL^{-1}$). (B) Kinetic data plotted as percent conversion from HPLC data. Optical density of the solution was measured at 600 nm. (C) Photographs of the initial micellar solution and at different time points showing the gradual formation of TBA hydrogel. (D) DLS graphs for mixed micelles (DBA-C6×4 – green, DBA-C6×3 – blue, and DBA-C6×2 – red) before the addition of PLE (solid lines), and the supernatant of the formulation after the complete macroscopic hydrogel formation (dotted lines).

hydrolyzed DBA becomes more hydrophilic and hence can no longer co-assemble into micelles, its capacity to stabilize the TBA in micellar form significantly diminishes. By overlaying the optical density and HPLC measurements, we observe that the TBA begins to coalesce into hydrogel macroparticle after 10 minutes when DBA-C6×2 concentration dropped to 60% of its initial level, marking the onset of cloudiness (Fig. 1B and C). Once the concentration of DBA-C6×2 decreased by around 90 percent, the TBA microparticles further coalesce and begin to collapse into hydrogel, after one hour of incubation with the activating enzyme, as depicted in Fig. 1C. Over time, this process progresses, causing the TBA to condense into bulk hydrogel and settle at the bottom of the HPLC vial as shown in Fig. 1C ($t$ = 12 h photo). As the coalescence and sedimentation of the TBA-based hydrogel occur gradually, the HPLC chromatogram continues to show a peak corresponding to TBA and relatively large error bars are obtained for this heterogenous sample, which is in transition from micellar to hydrogel mesophase, until the hydrogel drops below the HPLC needle sampling level and the mesophase transition is completed. At that point, the absence of the TBA peak in the chromatogram is not due to TBA hydrolysis but rather because the hydrogel has fallen below the needle sampling level. This was further corroborated by dissolving the TBA hydrogel in acetonitrile after gently removing the supernatant, and analyzing it with HPLC, which confirmed that the hydrogel was composed of TBA (with around 8% of partially hydrolyzed TBA out of the total TBA composition, Fig. S23†). To confirm the absence of micelles once the TBA hydrogel settled, the supernatant from the formulation was collected and analyzed using DLS. The DLS analysis (Fig. 1D – dotted red line) indicated the presence of only smaller species of diameters of 2–3 nm, which can be associated with the hydrolyzed DBA-C6×2 that was observed in the HPLC chromatogram (Fig. 1A). These observations align well with our previously reported findings, where we demonstrated that DBA hydrolyzes more rapidly than TBA, resulting in the formation of a TBA-based hydrogel upon selective enzymatic degradation of the DBA.[23,24]

### Characterization of the formed hydrogel

After confirming the ability of the mixed micellar formulation to transition into hydrogel mesophase upon enzymatic activation, we evaluated the mechanical properties of the precipitated hydrogel by conducting rheological measurements. The viscous-elastic region was determined through an amplitude sweep spanning from 0.01 to 100% at a frequency of 1 Hz. In the linear viscoelastic region (LVR) of this sample, the elastic modulus ($G'$) was higher than the viscous modulus ($G''$), which exhibited a distinct maximum at a higher strain value (Fig. 2). The amplitude sweep test confirmed that the TBA-based hydrogels indeed exhibit gel-like behavior, and are in good agreement with our recent reports on other hydrogels formed by these programmed mesophase transitions.[23,24] To further characterize the TBA based hydrogel, we used small-angle X-ray scattering (SAXS). The resulting patterns revealed that the scattering was primarily dominated by a single structure-factor correlation peak, representing the average distance between two cross-linking points in the hydrogel. This distance was determined to be 18 nm, aligning with the anticipated length of the TBA (Fig. S25†), and correlates well with previously reported data.[24] Additionally, a high-resolution scanning electron microscopy (HRSEM) image of the freeze-dried hydrogel displayed a highly porous structure, further supporting the formation of a hydrogel (Fig. S26†).

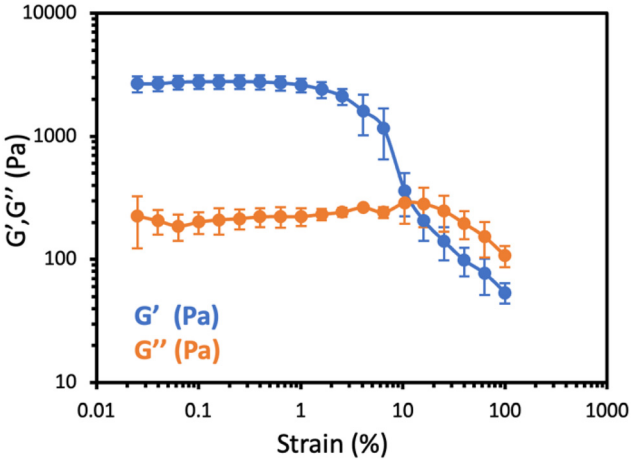


Fig. 2 Amplitude sweep test of the hydrogels obtained from 2 : 1 DBA-C6×2 (10 mg mL$^{-1}$) and TBA (5 mg mL$^{-1}$), at a constant frequency of 1 Hz.

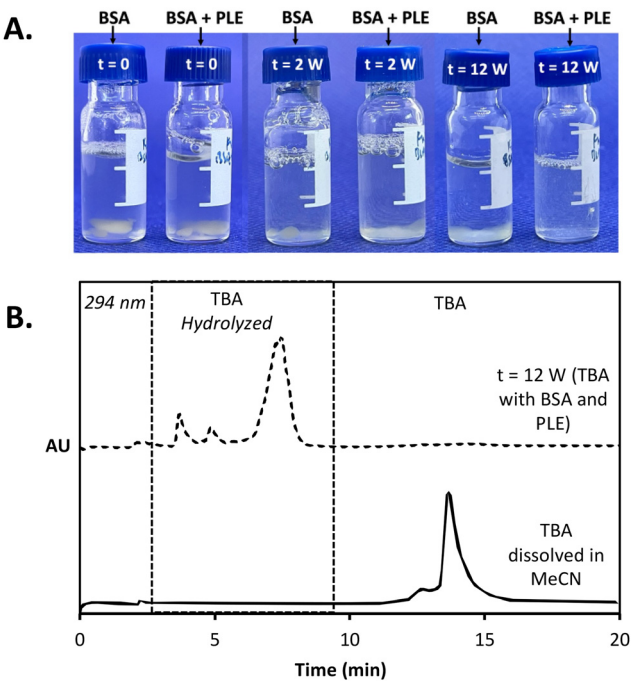


Fig. 3 (A) Photos of samples during the hydrolysis of TBA based hydrogel overtime in the presence of BSA (30 mg mL$^{-1}$) and, BSA and PLE (BSA = 30 mg ml$^{-1}$, PLE = 25 mg mL$^{-1}$). (B) HPLC chromatogram showing the complete hydrolysis of TBA after 12 weeks.

### Hydrogel to soluble polymer transition

The TBA-based hydrogel was designed to undergo further enzymatic degradation by cleavage of its hydrophobic hexanoate end-groups to yield water-soluble PEG-based polymers and hexanoic acid. Since no noticeable degree of degradation of the TBA was observed in parallel with the DBA-C6X2 degradation by PLE (PLE – 0.5 U $mL^{-1}$), we wished to expedite the hydrolysis of TBA-based hydrogel by using a higher concentration of PLE (25 U $mL^{-1}$) along with bovine serum albumin (BSA, 30 mg $mL^{-1}$). BSA is known to interact non-specifically with hydrophobic structures and can hence can tilt the unimer-aggregate equilibrium towards the unimer state,[44] thus allowing greater accessibility of the enzyme to the hydrophobic end-groups of the TBA. The solutions were incubated at 37 °C, and the degradation of the hydrogel was visually monitored over time (Fig. 3A). We observed that the hydrogel slowly disappeared from the bottom of the vial in the samples containing both PLE and BSA, while it could still be observed in the presence of only BSA. Once the TBA appeared to have completely disappeared (the transition from macro-gel to soluble polymers), we confirmed the full degradation of the TBA, by diluting the with acetonitrile and analyzing itwith HPLC, confirming the complete hydrolysis of TBA (Fig. 3B).

### Programming the time frame for hydrogel formation

After studying the ability of the DBA-C6×2 and TBA formulation to undergo the sequential mesophase transitions from micelles to hydrogel, and then eventually to fully degraded hydrophilic polymers, we wished to evaluate how would the hydrophobicity of the DBA component affect the first mesophase transition from micelles to hydrogel. Based on our previous studies of the enzymatic degradation rates of DBAs,[26,27] we expected that increasing the number of hydrophobic end-groups and thereby the hydrophobicity of the dendritic block, would lead to slower enzymatic hydrolysis of the DBA. Consequently, the time frame for the first mesophase transition would be extended.[26,45] The co-assembled micellar formulations using TBA and either DBA-C6×3 or DBA-C6×4 were prepared similarly to the DBA-C6×2 and TBA micelles, and PLE was added to the micellar solutions to study their first mesophase transition. For the DBA-C6×3 and TBA mixed micellar formulation (Fig. 4A), in the first 12 hours, the HPLC analysis

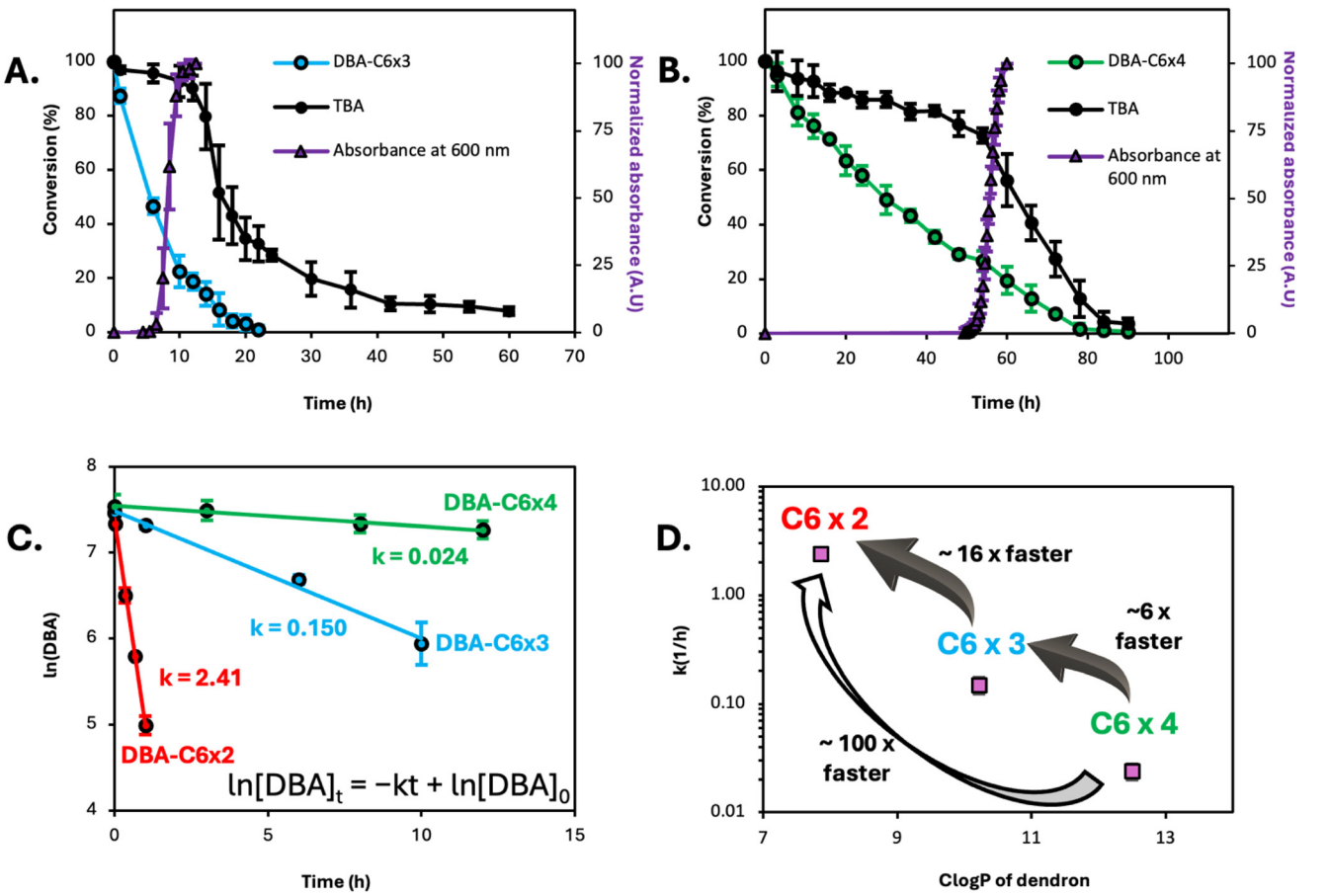


Fig. 4 Kinetic data plotted as percent conversion from HPLC data and optical density of the solution (measured at 600 nm) for the mesophase transition from micelles to hydrogel for mixed micellar formulations (DBA = 10 mg $mL^{-1}$, TBA = 5 mg $mL^{-1}$) in the presence of PLE (0.5 U $ml^{-1}$). (A) DBA-C6×3 and TBA mixed micellar formulation. (B) DBA-C6×4 and TBA mixed micellar formulation. (C) First order reaction rates of DBA hydrolysis in the mixed micellar formulation. (D) Logarithmic representation of the calculated rate constants plotted against the calculated log *P* (c log *P*, calculated by ChemDraw 22.0.0) values of the hydrophobic dendrons of the three DBAs.

 

showed the selective degradation of the DBA amphiphile and formation of the cleaved mPEG-triol, while the TBA remained nearly intact. Based on the turbidity measurements, we could see an increase in absorption after 6 hours, indicating that the TBA began to coalesce into microgels when the DBA-C6×3 concentration dropped to around 40% of its initial level. The increase in absorbance continued until it plateaued at 12 hours, when the DBA-C6×3 reached 20%, and in parallel, a sudden drop of almost 50% in the area of the HPLC peak corresponding to the TBA was observed, followed by a gradual decrease in its area over several days. Importantly, we didn't observe the formation of a new peak corresponding to the hydrolyzed TBA, indicating that the decrease in the concentration of TBA is due to the precipitation of the TBAs-based hydrogel. Next, we studied the mesophase transition of the DBA-C6×4 and TBA formulation. HPLC analysis (Fig. 4B) showed a significantly slower degradation of the DBA component. Similar to the other two formulations, the enzymatic degradation was highly selective toward the DBA, with only 15% of TBA dropping out of the solution during the first 46 hours. The coalescence of TBA began when the DBA-C6×4 concentration reached 25% of its initial value, occurring between 50 and 60 hours. Subsequently, we observed a sharp decrease in the TBA concentration, indicating its transition into a hydrogel mesophase. Since the transition from micelles to hydrogel evidently depends on the hydrolysis rate of the stabilizing DBA, we calculated the reaction kinetics of DBA hydrolysis. Assuming a pseudo first-order reaction $\ln[\mathrm{DBA}]_t = -kt + \ln[\mathrm{DBA}]_0$, we obtained linear fit and determined the rate of DBA hydrolysis from the slope of the natural logarithm of the DBA consumed over time (Fig. 4C). As the micelle-to-unimer equilibrium depends on the hydrophilic-lipophilic ratio of the amphiphiles, it could be directly correlated with the hydrophobicity of the DBA dendrons as all three had similar hydrophilic PEG block. With that in mind, we plotted the Clog $P$ of the dendrons (calculated by ChemDraw 22.0.0), as an estimate for the degree of hydrophobicity of the DBAs, against their respective DBA hydrolysis rate in the presence of PLE (Fig. 4D). Most interestingly, when comparing the hydrolysis rates for all three formulations, we found that DBA-C6×2 hydrolyzes approximately 16 times faster compared to DBA-C6×3, which, in turn, hydrolyzes approximately 6 times faster than DBA-C6×4. This significant change in hydrolysis rate is achieved solely by precisely adjusting the number of dendritic end-groups in the DBA, through molecular engineering of the dendritic branching unit. These results suggest that the rate of mesophase transitions can be tailored by changing the relative hydrophobicity of the stabilizing DBA through precise changes of the architecture of the DBA.

## Conclusions

The ability to program cascades of enzymatically induced sequential transition of polymeric assemblies between several mesophases has mostly relied on the incorporation of different enzymatic substrates into the polymeric backbone. Recently, we demonstrated the ability to program such sequential transitions by using molecular architecture as a programming tool. Building upon our recent report, in which we used the ratio between di- and tri-block amphiphiles as a tool for controlling the rate of mesophase transition from micelles to hydrogel, we demonstrate herein the introduction of an additional programming tool – the hydrophobicity of the di-block amphiphiles. Applying molecular engineering, we synthesized dendritic di-block amphiphiles with increasing number of enzymatically cleavable hydrophobic end-groups. We then made micellar formulations by co-assembling dendritic hydrogel-forming TBA, which possess esterase-responsive groups within its hydrophobic blocks, and the different DBAs, which functioned as a stabilizing agent for the micellar mesophase of the TBA. The transition from micelles to a hydrogel was initiated by introducing an esterase as the activating enzyme, which selectively cleaved the DBA monomers, due to their faster unimer-micelle-exchange rate, resulting in the mesophase transition of the TBA into hydrogel overtime. Importantly, we show that the rate of the transition from micelles to hydrogels could be tuned by altering the number of dendritic arms in the stabilizing DBA. Notably, DBA-C6×2, which possesses two arms, exhibited a hydrolysis rate approximately 100 times faster than DBA-C6×4, which has four arms, enabling the DBA-C6×2 based formulation to form hydrogels at a much faster rate compared to the formulation with DBA-C6×4. This finding underscores the significant impact of utilizing dendritic architecture as a tool for tuning the rate of mesophase transitions. In summary, our work demonstrates the potential to use molecular engineering to program the transformation of nano-micellar formulations into macroscopic hydrogels as well as their time frame. Future research endeavors may focus on further refining the properties of these hydrogels to cater to specific requirements in drug delivery and therapeutic applications. These results open up promising avenues for innovation in responsive materials.

## Author contributions

K.V. and R.J.A conceived and designed the project. P.R. and K. V. conducted rheology measurements. N.E-P. imaged the formed hydrogels by SEM. N.E-P., G.K. and R.B. measured and analyzed the SAXS data. S.T. and K.V. analyzed the NMR data and wrote the Experimental section. K.V. and R.J.A. wrote the manuscript, and all authors revised the final version.

## Data availability

The data supporting this article have been included as part of the ESI.†

## Conflicts of interest

There are no conflicts to declare.

## Acknowledgements

R. J. A. thanks the Israel Science Foundation (Grant 413/22) for the support of this research. R. B. thanks the Israel Science Foundation (1454/20) for the support of this research. K. V. thanks the Analytical Technologies Unit R&D, Kfar Saba, Teva, 4420909, Israel for the partial financial support. S. T. thanks the ADAMA Center for Novel Delivery Systems in Crop Protection, Tel-Aviv University, for the financial support.

## References

1 M. A. C. Stuart, W. T. S. Huck, J. Genzer, M. Müller, C. Ober, M. Stamm, G. B. Sukhorukov, I. Szleifer, V. V. Tsukruk, M. Urban, F. Winnik, S. Zauscher, I. Luzinov and S. Minko, Emerging Applications of Stimuli-Responsive Polymer Materials, *Nat. Mater.*, 2010, **9**(2), 101–113, DOI: **10.1038/nmat2614**.

2 M. Wei, Y. Gao, X. Li and M. J. Serpe, Stimuli-Responsive Polymers and Their Applications, *Polym. Chem.*, 2017, 127–143, DOI: **10.1039/c6py01585a**.

3 M.-F. Tsai, Y.-L. Lo, Y. Soorni, C.-H. Su, S. S. Sivasoorian, J.-Y. Yang and L.-F. Wang, Near-Infrared Light-Triggered Drug Release from Ultraviolet- and Redox-Responsive Polymersome Encapsulated with Core–Shell Upconversion Nanoparticles for Cancer Therapy, *ACS Appl. Bio Mater.*, 2021, **4**(4), 3264–3275, DOI: **10.1021/acsabm.0c01621**.

4 C. Song, F. Yang, R. Ji, Y. Lv and Z. Wei, Construction of a Drug Delivery System via PH-Responsive Polymeric Nanomicelles Containing Ferrocene for DOX Release and Enhancement of Therapeutic Effects, *ACS Omega*, 2021, **6**(42), 28242–28253, DOI: **10.1021/acsomega.1c04330**.

5 F. Hu, B. Liu, H. Chu, C. Liu, Z. Li, D. Chen and L. Li, Real-Time Monitoring of PH-Responsive Drug Release Using a Metal-Phenolic Network-Functionalized Upconversion Nanoconstruct, *Nanoscale*, 2019, **11**(18), 9201–9206, DOI: **10.1039/C9NR01892A**.

6 I. Rosenbaum, R. Avinery, A. J. Harnoy, G. Slor, E. Tirosh, U. Hananel, R. Beck and R. J. Amir, Reversible Dimerization of Polymeric Amphiphiles Acts as a Molecular Switch of Enzymatic Degradability, *Biomacromolecules*, 2017, **18**(10), 3457–3468, DOI: **10.1021/acs.biomac.7b01150**.

7 A. Klaikherd, C. Nagamani and S. Thayumanavan, Multi-Stimuli Sensitive Amphiphilic Block Copolymer Assemblies, *J. Am. Chem. Soc.*, 2009, **131**(13), 4830–4838, DOI: **10.1021/ja809475a**.

8 Z. Zhou, K. Maxeiner, D. Y. W. Ng and T. Weil, Polymer Chemistry in Living Cells, *Acc. Chem. Res.*, 2022, **55**(20), 2998–3009, DOI: **10.1021/ACS.ACCOUNTS.2C00420/ASSET/IMAGES/LARGE/AR2C00420_0007.JPEG**.

9 M. Nakahata, Y. Takashima, H. Yamaguchi and A. Harada, Redox-Responsive Self-Healing Materials Formed from Host–Guest Polymers, *Nat. Commun.*, 2011, **2**(1), 511, DOI: **10.1038/ncomms1521**.

10 H. Kitajima, S. Ida, S. Bhowmik, S. Yusa and S. Kanaoka, PH-Responsive, Aggregation Control of Multiarm Star Polymers Depending on the Ionic Segment Sequence of Arm Polymers, *Polym. J.*, 2022, **54**(5), 715–725, DOI: **10.1038/s41428-022-00621-3**.

11 J. F. Quinn, M. R. Whittaker and T. P. Davis, Glutathione Responsive Polymers and Their Application in Drug Delivery Systems, *Polym. Chem.*, 2017, **8**(1), 97–126, DOI: **10.1039/C6PY01365A**.

12 A. J. Harnoy, I. Rosenbaum, E. Tirosh, Y. Ebenstein, R. Shaharabani, R. Beck and R. J. Amir, Enzyme-Responsive Amphiphilic PEG-Dendron Hybrids and Their Assembly into Smart Micellar Nanocarriers, *J. Am. Chem. Soc.*, 2014, **136**(21), 7531–7534, DOI: **10.1021/ja413036q**.

13 J. Xie, S. Tian, H. Zhang, C. Feng, Y. Han, H. Dai and L. Yan, A Novel NQO1 Enzyme-Responsive Polyurethane Nanocarrier for Redox-Triggered Intracellular Drug Release, *Biomacromolecules*, 2023, **24**(5), 2225–2236, DOI: **10.1021/acs.biomac.3c00134**.

14 S. Kashyap, N. Singh, B. Surnar and M. Jayakannan, Enzyme and Thermal Dual Responsive Amphiphilic Polymer Core–Shell Nanoparticle for Doxorubicin Delivery to Cancer Cells, *Biomacromolecules*, 2016, **17**(1), 384–398, DOI: **10.1021/acs.biomac.5b01545**.

15 C. E. Callmann, C. V. Barback, M. P. Thompson, D. J. Hall, R. F. Mattrey and N. C. Gianneschi, Therapeutic Enzyme-Responsive Nanoparticles for Targeted Delivery and Accumulation in Tumors, *Adv. Mater.*, 2015, **27**(31), 4611–4615, DOI: **10.1002/adma.201501803**.

16 M. T. Proetto, C. E. Callmann, J. Cliff, C. J. Szymanski, D. Hu, S. B. Howell, J. E. Evans, G. Orr and N. C. Gianneschi, Tumor Retention of Enzyme-Responsive Pt(II) Drug-Loaded Nanoparticles Imaged by Nanoscale Secondary Ion Mass Spectrometry and Fluorescence Microscopy, *ACS Cent. Sci.*, 2018, **4**(11), 1477–1484, DOI: **10.1021/acscentsci.8b00444**.

17 G. Slor, A. R. Olea, S. Pujals, A. Tigrine, V. R. De La Rosa, R. Hoogenboom, L. Albertazzi and R. J. Amir, Judging Enzyme-Responsive Micelles by Their Covers: Direct Comparison of Dendritic Amphiphiles with Different Hydrophilic Blocks, *Biomacromolecules*, 2021, **22**(3), 1197–1210, DOI: **10.1021/acs.biomac.0c01708**.

18 M. Segal, L. Ozery, G. Slor, S. S. Wagle, T. Ehm, R. Beck and R. J. Amir, Architectural Change of the Shell-Forming Block from Linear to V-Shaped Accelerates Micellar Disassembly, but Slows the Complete Enzymatic Degradation of the Amphiphiles, *Biomacromolecules*, 2020, **21**(10), 4076–4086, DOI: **10.1021/acs.biomac.0c00882**.

19 J. Gao, J. Zhan and Z. Yang, Enzyme-Instructed Self-Assembly (EISA) and Hydrogelation of Peptides, *Adv. Mater.*, 2020, **32**(3), 1805798, DOI: **10.1002/adma.201805798**.

20 H. Wang, Z. Feng, D. Wu, K. J. Fritzsching, M. Rigney, J. Zhou, Y. Jiang, K. Schmidt-Rohr and B. Xu, Enzyme-Regulated Supramolecular Assemblies of Cholesterol Conjugates against Drug-Resistant Ovarian Cancer Cells,

 

*J. Am. Chem. Soc.*, 2016, **138**(34), 10758–10761, DOI: **10.1021/jacs.6b06075**.

21 M. P. Chien, A. M. Rush, M. P. Thompson and N. C. Gianneschi, Programmable Shape-Shifting Micelles, *Angew. Chem., Int. Ed.*, 2010, **49**, 5076–5080, DOI: **10.1002/anie.201000265**.

22 T.-H. H. Ku, M.-P. P. Chien, M. P. Thompson, R. S. Sinkovits, N. H. Olson, T. S. Baker and N. C. Gianneschi, Controlling and Switching the Morphology of Micellar Nanoparticles with Enzymes, *J. Am. Chem. Soc.*, 2011, **133**, 8392–8395, DOI: **10.1021/ja2004736**.

23 P. Rathee, N. Edelstein-Pardo, F. Netti, L. Adler-Abramovich, A. Sitt and R. J. Amir, Architecture-Based Programming of Polymeric Micelles to Undergo Sequential Mesophase Transitions, *ACS Macro Lett.*, 2023, **12**(6), 814–820, DOI: **10.1021/ACSMACROLETT.3C00153/ASSET/IMAGES/LARGE/MZ3C00153_0004.JPEG**.

24 P. Rathee, N. Edelstein-Pardo, G. Koren, R. Beck and R. J. Amir, Cascade Mesophase Transitions of Multi-Enzyme Responsive Polymeric Formulations, *Biomacromolecules*, 2024, **25**(6), 3607–3619, DOI: **10.1021/acs.biomac.4c00221**.

25 G. Slor and R. J. Amir, Using High Molecular Precision to Study Enzymatically Induced Disassembly of Polymeric Nanocarriers: Direct Enzymatic Activation or Equilibrium-Based Degradation?, *Macromolecules*, 2021, **54**(4), 1577–1588, DOI: **10.1021/acs.macromol.0c02263**.

26 M. Segal, R. Avinery, M. Buzhor, R. Shaharabani, A. J. Harnoy, E. Tirosh, R. Beck and R. J. Amir, Molecular Precision and Enzymatic Degradation: From Readily to Undegradable Polymeric Micelles by Minor Structural Changes, *J. Am. Chem. Soc.*, 2017, **139**(2), 803–810, DOI: **10.1021/jacs.6b10624**.

27 A. J. Harnoy, M. Buzhor, E. Tirosh, R. Shaharabani, R. Beck and R. J. Amir, Modular Synthetic Approach for Adjusting the Disassembly Rates of Enzyme-Responsive Polymeric Micelles, *Biomacromolecules*, 2017, **18**(4), 1218–1228, DOI: **10.1021/acs.biomac.6b01906**.

28 M. J. Mitchell, M. M. Billingsley, R. M. Haley, M. E. Wechsler, N. A. Peppas and R. Langer, Engineering Precision Nanoparticles for Drug Delivery, *Nat. Rev. Drug Discovery*, 2020, **20**(2), 101–124, DOI: **10.1038/s41573-020-0090-8**.

29 M. Panagi, F. Mpekris, P. Chen, C. Voutouri, Y. Nakagawa, J. D. Martin, T. Hiroi, H. Hashimoto, P. Demetriou, C. Pierides, R. Samuel, A. Stylianou, C. Michael, S. Fukushima, P. Georgiou, P. Papageorgis, P. C. Papaphilippou, L. Koumas, P. Costeas, G. Ishii, M. Kojima, K. Kataoka, H. Cabral and T. Stylianopoulos, Polymeric Micelles Effectively Reprogram the Tumor Microenvironment to Potentiate Nano-Immunotherapy in Mouse Breast Cancer Models, *Nat. Commun.*, 2022, **13**(1), 7165, DOI: **10.1038/s41467-022-34744-1**.

30 A. Chaudhuri, K. Ramesh, D. N. Kumar, D. Dehari, S. Singh, D. Kumar and A. K. Agrawal, Polymeric Micelles: A Novel Drug Delivery System for the Treatment of Breast Cancer, *J. Drug Delivery Sci. Technol.*, 2022, **77**, 103886, DOI: **10.1016/j.jddst.2022.103886**.

31 D. A. Prince, I. J. Villamagna, A. Borecki, F. Beier, J. R. de Bruyn, M. Hurtig and E. R. Gillies, Thermoresponsive and Covalently Cross-Linkable Hydrogels for Intra-Articular Drug Delivery, *ACS Appl. Bio Mater.*, 2019, **2**(8), 3498–3507, DOI: **10.1021/acsabm.9b00410**.

32 T. Yeruva, S. Yang, S. Doski and G. A. Duncan, Hydrogels for Mucosal Drug Delivery, *ACS Appl. Bio Mater.*, 2023, **6**(5), 1684–1700, DOI: **10.1021/acsabm.3c00050**.

33 G. Thamilselvan, H. David, A. Sajeevan, S. Rajaramon, A. P. Solomon, R. D. Durai and V. H. B. Narayanan, Polymer Based Dual Drug Delivery System for Targeted Treatment of Fluoroquinolone Resistant Staphylococcus Aureus Mediated Infections, *Sci. Rep.*, 2023, **13**(1), 11373, DOI: **10.1038/s41598-023-38473-3**.

34 R. Zhong, S. Talebian, B. B. Mendes, G. Wallace, R. Langer, J. Conde and J. Shi, Hydrogels for RNA Delivery, *Nat. Mater.*, 2023, **22**(7), 818–831, DOI: **10.1038/s41563-023-01472-w**.

35 A. K. Mahanta and P. Maiti, Injectable Hydrogel through Hydrophobic Grafting on Chitosan for Controlled Drug Delivery, *ACS Appl. Bio Mater.*, 2019, **2**(12), 5415–5426, DOI: **10.1021/acsabm.9b00733**.

36 D. Das and S. Pal, Modified Biopolymer-Dextrin Based Crosslinked Hydrogels: Application in Controlled Drug Delivery, *RSC Adv.*, 2015, **5**(32), 25014–25050, DOI: **10.1039/C4RA16103C**.

37 L. H. Nguyen, M. Gao, J. Lin, W. Wu, J. Wang and S. Y. Chew, Three-Dimensional Aligned Nanofibers-Hydrogel Scaffold for Controlled Non-Viral Drug/Gene Delivery to Direct Axon Regeneration in Spinal Cord Injury Treatment, *Sci. Rep.*, 2017, **7**(1), 42212, DOI: **10.1038/srep42212**.

38 W. He, M. Reaume, M. Hennenfent, B. P. Lee and R. Rajachar, Biomimetic Hydrogels with Spatial- and Temporal-Controlled Chemical Cues for Tissue Engineering, *Biomater. Sci.*, 2020, **8**(12), 3248–3269, DOI: **10.1039/D0BM00263A**.

39 J. Mayr, C. Saldías and D. Díaz Díaz, Release of Small Bioactive Molecules from Physical Gels, *Chem. Soc. Rev.*, 2018, **47**(4), 1484–1515, DOI: **10.1039/C7CS00515F**.

40 A. J. Harnoy, N. Papo, G. Slor and R. J. Amir, Mixing End Groups in Thiol-Ene/Yne Reactions as a Simple Approach toward Multienzyme-Responsive Polymeric Amphiphiles, *Synlett*, 2018, **29**(19), 2582–2587, DOI: **10.1055/s-0037-1611340**.

41 T. O. Machado, C. Sayer and P. H. H. Araujo, Thiol-Ene Polymerisation: A Promising Technique to Obtain Novel Biomaterials, *Eur. Polym. J.*, 2017, **86**, 200–215, DOI: **10.1016/j.eurpolymj.2016.02.025**.

42 R. Hoogenboom, Thiol-Yne Chemistry: A Powerful Tool for Creating Highly Functional Materials, *Angew. Chem., Int. Ed.*, 2010, **49**, 3415–3417, DOI: **10.1002/anie.201000401**.

43 A. Fernandez, C. A. Zentner, M. Shivrayan, E. Samson, S. Savagatrup, J. Zhuang, T. M. Swager and

S. Thayumanavan, Programmable Emulsions via Nucleophile-Induced Covalent Surfactant Modifications, *Chem. Mater.*, 2020, **32**(11), 4663–4671, DOI: **10.1021/acs.chemmater.0c01107**.

44 N. Feiner-Gracia, M. Buzhor, E. Fuentes, S. S. Pujals, R. J. Amir and L. Albertazzi, Micellar Stability in Biological Media Dictates Internalization in Living Cells, *J. Am. Chem. Soc.*, 2017, **139**(46), 16677–16687, DOI: **10.1021/jacs.7b08351**.

45 R. J. Amir and S. Tevet, Hydrophobicity as a Tool for Programming Sequential Mesophase Transitions of Enzyme-Responsive Polymeric Amphiphiles, *J. Mater. Chem. B*, 2024, **12**, 11685–11695, DOI: **10.1039/D4TB01587H**.